American Mineralogist, Volume 76, pages 1563–1579, 1991

The bound interlayer H_2O content of potassic white micas: Muscovite-hydromuscovite-hydropyrophyllite solutions

Robert R. Loucks

Ore Petrology–Geochemistry Program, Department of Earth and Atmospheric Sciences, Purdue University, West Lafayette, Indiana 47907, U.S.A.

Abstract

High-quality chemical analyses of potassic white micas usually show an apparent deficit of cations (K, Na, Rb, Cs, NH_4, Ca, Sr, Ba) in 12-coordinated interlayer sites. The stoichiometric deficit has been widely attributed to the substitution $^{[4]}Al + {}^{[12]}K = {}^{[4]}Si + {}^{[12]}\square$ ($\square$ = vacancy), in which the right hand side represents a pyrophyllite-like molecular component that is supposedly prevalent in illite. If the sites presumed vacant are not vacant, there are important consequences to sedimentary, hydrothermal, and metamorphic petrology.

From the literature, 72 superior wet-chemical analyses of muscovite, lepidolite, and single-phase illites have been compiled. These analyses report $H_2O(+)$, $H_2O(-)$, Fe_2O_3, FeO, halogens (in most cases), minor alkalis, and alkaline earth elements; they have analysis totals in the range 99.5–100.5 wt%. The molar proportion of structurally bound H_2O, $H_2O(+)$, shows a strong negative correlation with the sum K + Na + Rb + Cs + Ca + Ba + 0.33(F + Cl), which demonstrates that the $H_2O(+)$ excess over that required for full occupancy of halogen-OH sites is chiefly bound in interlayer sites of alkali-deficient micas. To interpret its crystal-chemical significance, an analysis of the components of variance in measured $H_2O(+)$ content proceeds by statistically testing three models for incorporation of H_2O in interlayer sites: (1) as neutral H_2O molecules, (2) as hydronium ions, H_3O^+, and (3) as a combination of H_2O and H_3O^+. Only the third provides a statistically satisfactory description of the observed variations in white mica chemical composition and, in fact, accounts for all the observed covariation of molar $H_2O(+)$ with the sum K + Na + Rb + Cs + Ca + Ba + 0.33(F + Cl). None of the variance in interlayer site composition is statistically associable with interlayer vacancies. This test establishes that the commonly inferred occurrence of vacant interlayer sites is virtually nonexistent. The supposed vacancies are occupied by hydronium ions and H_2O molecules having partial molar enthalpy and entropy contributions that significantly enhance the low-temperature thermodynamic stability of H_2O-rich illitic and sericitic micas and probably glauconite as well.

A number of papers in recent years have inferred that illite is metastable with respect to a mechanical mixture of muscovite (or phengite) plus pyrophyllite; the reasoning was that illite compositions were inferred to lie well within the muscovite-pyrophyllite miscibility gap and have been shown to decompose into interlaminated muscovite plus pyrophyllite upon heating. That argument for illite metastability is false because $Al_2Si_4O_{10}(OH)_2$ is not a significant molecular component of illite crystalline solutions. A revised topology of phase relations for coexisting white mica and aluminum silicates is presented.

Preliminary data indicate that H_3O^+ is liberated chiefly between 250 and 500 °C, whereas OH sites dehydrate above 500 °C. Because the interlayer commonly contains 15–30% of the total bound H_2O in micas formed below about 450 °C, experimental calibrations of H and O isotopic fractionation factors between micas and other phases (as well as routine isotopic analyses of natural micas from hydrothermal, low-grade metamorphic and sedimentary parageneses) must utilize H_2O extraction methods that take account of structurally bound H_2O in interlayer as well as OH sites. Upon calibration, O and H isotope partitioning between OH and interlayer sites may serve as an intracrystalline isotope thermometer or cooling rate speedometer. Pending experimental calibration, the interlayer hydronium proportion may be used as an f_{H_2O} barometer for metamorphic environments and as a pH meter for hydrothermal environments.

0003–004X/91/0910–1563$02.00

Introduction

It is well established on the basis of X-ray and neutron diffraction studies (Lundgren and Olovsson, 1976) and infrared, Raman, and NMR spectroscopic studies (Williams, 1976) that the crystalline monohydrates of many inorganic and some organic acids (e.g., nitric, sulfuric, perchloric, hydrofluoric, hydrochloric, hydrobromic, hydroiodic) are in fact hydronium (= oxonium) salts corresponding to formulas of the type $(H_3O)Cl$ and $(H_3O)ClO_4$, rather than $HCl \cdot H_2O$ and $HClO_4 \cdot H_2O$. These diffraction and spectroscopic studies demonstrate that, like the isoelectronic H_3N ammonia molecule, the H_3O^+ ion has C_{3V} pyramidal symmetry in which all H atoms are essentially equivalent in O-H bond length and orientation. The diffraction studies have shown that the simple hydronium salt crystals are in nearly all cases isostructural with the corresponding ammonium salt, because they have similar structures and the crystallographic ionic radius of H_3O^+ is only about 3.4% smaller than that of H_4N^+ (Ito et al., 1987). Because H_3O^+ is only about 5% larger than the K^+ ion, most hydronium and ammonium salts are isostructural with the potassium salt as well. The substitution of ammonium for K in natural and synthetic micas, feldspars, and zeolites is well established (Barrer and Denny, 1961; Barker, 1964; Erd et al., 1964; Hallam and Eugster, 1976; Honma and Itihara, 1981; Sterne et al., 1982; Higashi, 1982; Hori et al., 1986). These relations invite the supposition that hydronium analogues of all known ammonium aluminosilicates (micas, feldspars, zeolites) probably exist, if not as pure compounds, then at least as molecular components in crystalline solutions. Apropos of this point is a natural, hydrothermal *1M* tobelite described by Higashi (1982), for which differential thermogravimetric analysis showed 6.40 wt% structurally bound water, $H_2O(+)^{105°C}$. Employing the procedure introduced herein for recasting mica chemical analyses as charge-balanced structural formulas, Higashi's wet-chemical analysis corresponds to a nearly ideally stoichiometric dioctahedral ammonium-hydronium mica: $[(H_4N)_{0.526}(H_3O)_{0.212}(H_2O)_{0.069}K_{0.191}Na_{0.005}]_{1.003}(Al_{1.921}Mg_{0.050}Fe^{2}_{0.028}Ti_{0.001})_{2.000}(Al_{0.856}Si_{3.144})_{4.000}O_{10}(OH)_{2.000}$.

Previously reported evidence for interlayer hydronium

Differential thermogravimetric analysis

Kodama and Brydon (1968) used a sedimentation technique to divide a very fine-grained, single-phase, $2M_1$ sericite from a Japanese hydrothermal ore deposit into six fractions of natural grain size, ranging from 0.2 to 20 μm (median 4 μm). Precise wet-chemical analyses of each size fraction showed no significant compositional variation over the range 20–5 μm, but the three finest size fractions showed a substantial enrichment in $H_2O(+)^{110°C}$ and a depletion in K_2O that is partially, but not fully, charge compensated by $SiAl_{-1}$ substitution in tetrahedral sites. Cation proportions in the four finest size fractions, normalized to six octahedral + tetrahedral cations, are:

5–2 μm: $(K,Na,Ca)_{0.92}[(Al,Fe^{3+},Ti)_{1.96}(Mg,Fe^{2+})_{0.04}]_{2.00}(Al_{0.96}Si_{3.04})_{4.00}$ with 1.04 mol $H_2O(+)$

2–1 μm: $(K,Na,Ca)_{0.89}[(Al,Fe^{3+},Ti)_{1.96}(Mg,Fe^{2+})_{0.04}]_{2.00}(Al_{0.95}Si_{3.05})_{4.00}$ with 1.05 mol $H_2O(+)$

1–0.5 μm: $(K,Na,Ca)_{0.84}[(Al,Fe^{3+},Ti)_{1.96}(Mg,Fe^{2+})_{0.04}]_{2.00}(Al_{0.92}Si_{3.08})_{4.00}$ with 1.14 mol $H_2O(+)$

0.5–0.2 μm: $(K,Na,Ca)_{0.82}[(Al,Fe^{3+},Ti)_{1.96}(Mg,Fe^{2+})_{0.04}]_{2.00}(Al_{0.89}Si_{3.11})_{4.00}$ with 1.42 mol $H_2O(+)$.

Differential thermogravimetric analysis (DTGA, measurements of weight loss at 10 °C increments) from 110 to 1000 °C showed no major weight loss below 500 °C for size fractions >1 μm and complete dehydroxylation over the 500–700 °C interval (peaking at ~600 °C). The two more hydrous fine fractions <1 μm showed an additional pronounced peak in H_2O loss rate at around 270 °C, although the finest fraction additionally underwent slower but steady loss of ~0.12 mol H_2O per mole of mica over the 110–230 °C interval.

Mica flakes 0.2 μm in diameter have a molar surface area on the order of 30000 m^2, and increasing the surface area may lead to an increase in adsorbed H_2O as interlayer cations exposed at the surface become hydrated and a corresponding decrease in K_2O content with increasing surface area because exposed K^+ ions are leachable; these factors probably account for much of Kodama and Brydon's reported excess of $H_2O(+)$ that was released gradually by the <0.5-mm size fraction during heating from 110 to 230 °C. Norrish and Pickering (1983) have noted that it is difficult to determine the structural H_2O content of pedogenic illite (mostly <1 μm) because H_2O is lost continuously with heating, and there is no recognizable hiatus that divides structural from hygroscopic H_2O. However, Kodama and Brydon's pronounced DTGA peak around 250–300 °C in hydrothermal sericite must correspond to loss of structurally bound H_2O from a particular kind of lattice site that has distinctive H_2O binding energies different from OH sites because the other sharp, major peak in weight loss rate at 600–660 °C in all size fractions is plainly caused by dehydroxylation (Guggenheim et al., 1987).

H isotope exchange kinetics

Moum and Rosenqvist (1958) dried a sample of illite at 110 °C and sealed numerous 10-g aliquots in silica tubes together with 1 g of deuterium-rich water. The tubes were heated in ovens at 110 °C for lengths of time ranging from minutes to 610 d, and the products were analyzed to determine the isotopic exchange rate. Their plot of percent exchange vs. time resembles a three-step staircase, which they interpret as radically different exchange rates for three structurally distinct modes of occurrence of H_2O in the illite: (1) a fraction (13%) that reaches exchange equilibrium with the wetting solution in a period of hours, which

they ascribe to adsorbed H_2O that was not liberated by drying at 110 °C; (2) a fraction (17%) with higher lattice binding energy that reaches exchange equilibrium with the wetting solution in a period of 6–12 weeks, which they ascribe to hydronium in interlayer sites; and (3) a fraction (~70%) that is little changed in experimental times approaching 2 yr, which they ascribe to OH groups.

Spectroscopy

Infrared (IR) spectroscopic studies aimed at discriminating hydronium ions from H_2O molecules in minerals and synthetic inorganic compounds and aqueous acids have been reviewed by Wilkins et al. (1974), Williams (1976), and Ripmeester et al. (1986). In the last paper, hydronium in alunite and jarosite was confirmed conclusively on deuterated samples by nuclear magnetic resonance spectroscopy with magic angle spinning. Wilkins et al. (1974) employed IR spectroscopy to confirm hydronium in uranospinite. White and Burns (1963) and Sclar et al. (1965) reported recognition of hydronium in muscovite and in the synthetic high-pressure mica- or talc-like compound $(H_3O)_2Mg_5Si_8O_{20}(OH)_4$, but these last two reports have been met with skepticism because in crystals the IR spectrum of H_3O^+ is distinguished from that of H_2O by the presence of O-H bending modes at frequencies around 1050–1100 cm^{-1} (Williams, 1976). However, these frequencies overlap those of OH groups, so in the presence of OH it has not been possible to demonstrate the presence of hydronium by currently available IR (or Raman) spectroscopic techniques on undeuterated samples.

Other methods

In an abstract providing no procedural details, Hervig and Peacock (1989) report results of ion microprobe analyses of H in muscovite and biotite in pelitic schists that showed a common excess of H over the stoichiometric requirement to fill OH sites. They assigned the excess H to interlayer sites as hydronium, which resulted in full occupancy of these sites in all muscovite and nearly full occupancy in the biotite.

Dyar (1988) used fast neutron activation analysis to measure directly the O content of biotite in metapelites. Her abstract reports a stoichiometric excess of O that correlates with a deficit of interlayer alkali and alkaline earth cations, so she assigned the excess O to interlayer sites as hydronium to improve the charge balance.

Prior interpretations of interlayer cation deficit and H_2O excess in muscovite and illite

Interlayer vacancies

It has long been noted that high-quality wet-chemical and electron microprobe analyses of potassic white micas (muscovite, sericite, phengite, celadonite, illite) usually have an apparent deficiency of large cations (K, Na, Ca, Sr, Ba, Rb, Cs, NH_4) in the 12-coordinated interlayer sites relative to the stoichiometric ideal of one interlayer cation per $O_{10}(OH,F)_2$ in the standard formula (e.g., Lambert, 1959; Holdaway, 1980; Zen, 1981; Guidotti, 1984; Wang and Banno, 1987; Jiang et al., 1990). In conventional practice, these interlayer cations plus tetrahedral and octahedral cations are normalized to a total charge of +22, with the usual consequence of an apparent deficit of interlayer occupants that correlates with an apparent excess of octahedral cations over the two in ideal dioctahedral micas. In recent years, crystal-chemical and thermodynamic models of phengite and illite solid solutions consistently assume that interlayer sites not occupied by the listed cations are vacant (□) and are assignable to a pyrophyllite-like $\square Al_2Si_4O_{10}(OH)_2$ molecular component (e.g., Tardy and Fritz, 1981; Stoessel, 1981; Merino and Ransom, 1982; Aagaard and Helgeson, 1983; Garrells, 1984; Giggenbach, 1985; Helgeson and Aagaard, 1985; Wang and Banno, 1987; Baldelli et al., 1989).

Interlayer hydronium

An equally significant feature of white mica crystal chemistry that has received less attention is that most high-quality chemical analyses of potassic white micas in metamorphic, hydrothermal, and sedimentary rocks report a content of "structurally bound" H_2O in excess of the amount required for full occupancy of the two halogen-OH sites, which is 4.52 wt% for stoichiometrically ideal hydroxy-muscovite. Structurally bound H_2O, $H_2O(+)$, is defined as H_2O not liberated by heating to 105 ± 5 °C but released on further heating to ~1000 °C.

Citing the established precedent of solid solutions of jarosite-ammoniojarosite-hydronium jarosite $[(K^+, H_4N^+, H_3O^+)Fe_3(SO_4)_2(OH)_6]$ in nature, Brown and Norrish (1952) recommended that in exceptionally hydrous, alkali-deficient white micas, the analytical $H_2O(+)$ in excess of OH-site requirements may be assigned to interlayer sites as hydronium ion, H_3O^+. Their illustrative cases of two hydrothermal hydromuscovites and two pedogenic illites gave calculated structural formulas with interlayer H_3O^+ that approximated ideal dioctahedral mica stoichiometry much more closely than formulas that were calculated by ignoring "excess" H_2O or by assuming more OH groups and fewer unprotonated O atoms than the standard ideal formula. Brown and Norrish's recommendation was widely adopted until the late 1960s.

Interlayer H_2O molecules

Hower and Mowatt (1966) presented new wet-chemical analyses of 21 pedogenic and sedimentary illites and interlayered illite-smectite mixtures and compiled an additional six illite-smectite analyses from the literature. They calculated structural formulas of these clays by (1) assuming that the $H_2O(+)$ in excess of two OH groups per standard formula occurs as neutral H_2O molecules hydrating cations in interlayer sites and (2) normalizing the remaining cations to 22 positive charges to balance 11 O atoms. This practice normally resulted in a deficit of interlayer charge from K, Na, and Ca and an excess of Mg + Fe + Al + Si cations over the stoichiometric ideal of

six octahedral + tetrahedral cations per formula unit; the excess was relieved by (3) shifting Mg into interlayer sites as needed to balance the layer charge and interlayer charge. The last practice is acceptable for smectites and smectite layers in mixed-layer clays, but assigning Mg to interlayer positions to achieve layer charge balance in single-phase illites has not been justified. The 27 samples considered by Hower and Mowatt (1966) include only three for which XRD data indicate less than 10% interlayered smectite, and their chemical analyses have large errors, with totals ranging from 97.36 to 103.04 wt% (only five of which were 99.5–100.5%), with too much scatter and too few samples for a definitive test of structural-formula models of single-phase illite. They nevertheless asserted their preference for representation of "excess" $H_2O(+)$ as interlayer H_2O molecules rather than hydronium ion. Hower and Mowatt's (1966) model of illite and sericite as a solid solution chiefly of pyrophyllite, muscovite, and celadonite and without a hydronium-muscovite component has been widely adopted in the past two decades, although the justification was no more definitive than the proposal of Brown and Norrish (1952).

The chemical analysis data base

In this section, criteria are described for selection of published, superior-quality wet-chemical analyses of potassic white micas. In subsequent sections, these data are used to test statistically the fit of alternative models for calculating white mica structural formulas, focusing particularly on occupancy of interlayer sites and secondarily on the commonly reported excess of octahedral cations over the two appropriate for ideal dioctahedral micas.

The data base consists of 72 wet-chemical analyses of muscovite, lepidolite, and illite from igneous, metamorphic, low-pressure hydrothermal, and sedimentary environments (Appendix 1).[1] The criteria for selection are as follows: (1) analysis totals between 99.5 and 100.5 wt%; (2) a report of separately determined $H_2O(-)$ and $H_2O(+)$; (3) a report of separately determined FeO and Fe_2O_3 unless Fe_{tot} is <0.35 wt% Fe (two analyses lacking Fe^{2+} and Fe^{3+} determinations but having very low Fe_{tot} were accepted); (4) FeO + Fe_2O_3 < 5 wt% Fe_2O_3 equivalent because oxidation of FeO may result in OH deprotonation with increasing Fe content (Eugster and Wones, 1962); (5) a report of F content of micas from metamorphic and igneous environments because F-rich micas have not been reported from sedimentary and diagenetic environments, and experimental data show that in fluorite- or apatite-bearing parageneses, the relative importance of micas as halogen hosts increases with increasing temperature (Munoz and Ludington, 1974; Ludington, 1978) and a report of Li_2O in all micas having F > 0.5 wt% because Li and F contents tend to be correlated, e.g., Foster, 1964; (6) CaO analyzed; (7) CaO < 0.5 wt% because (a) Ca might be coupled with interlayer vacancies for local charge balance rather than coupled with Al as a margarite-type molecular component (Guidotti, 1984, p. 374), which contributes another uncertainty to calculation of structural formulas, and (b) elevated CaO was encountered chiefly in illite analyses, in which it may occur as a calcium beidellite component in an interstratified smectite phase; (8) sedimentary and pedogenic illites were not accepted unless X-ray diffraction studies on glycolated samples indicated them to be single-phase, a stipulation that resulted in rejection of most of the many illite analyses considered.

Five illite analyses met criteria 1–8, including two from the 27 presented by Hower and Mowatt (1966). All analyses of potassic white micas that met these eight criteria were included in the data set. The analyses come from four compilations published in the 1960s and 1970s and from ten additional primary sources.

Test for interlayer H_2O

For solutions of ideal end-member mica molecules in which interlayer sites are fully occupied by ions, H_2O can be gained or lost by the crystal structure by either of two substitution mechanisms: (1) alkali (or alkaline earth)–hydronium exchange and (2) halogen–OH exchange. (OH deprotonation accompanying Fe oxidation is ignored.) Along interlayer ion-exchange vectors of the type $K(H_3O)_{-1}$, the variation in moles of H_2O scales as $\partial n_K/\partial n_{H_2O} = 1/1.5 = 0.67$ (where n is the molar proportion), but along halogen-OH exchange vectors such as $F(OH)_{-1}$, H_2O varies as $\partial n_F/\partial n_{H_2O} = 2$, so condensation of compositional coordinates can be effected by multiplying the halogen exchange vector by one-third to make it colinear with the interlayer ion-exchange vector. In Figure 1, the molar proportion of structurally bound H_2O, $H_2O(+)$, is plotted against the molar proportion of conventional interlayer cations plus one-third of the halogens, all normalized to a number of octahedral and tetrahedral cations totaling 6 + 0.5 Li (atomic), as appropriate for solid solutions of trioctahedral lepidolite and dioctahedral, muscovite-like components. All stoichiometrically ideal di- and trioctahedral, OH and halogen micas (polylithionite, celadonite, fluorphlogopite, muscovite, hydronium-hydroxymica, hydronium-fluormica, etc.) plot along a straight line in these coordinates. The pyrophyllite, $\square Al_2Si_4O_{10}(OH)_2$, and hydropyrophyllite, $(H_2O)Al_2Si_4O_{10}(OH)_2$, components lie off the mica trend in directions indicated by arrows on Figure 1. All OH micas other than hydronium-hydroxylmica plot at the coordinates $x, y = 1, 1$; hydronium-fluormica, $(H_3O)Al_2AlSi_3O_{10}F_2$, plots at 0.67, 1.5; all other F analogues (fluormuscovite, fluorceladonite, etc.) plot at 1.67, 0. In a formula normalized to 22 positive charges from Al + Si per formula unit, kaolinite (not shown) would plot at 0, 3.14; X-ray diffraction studies of all samples from low-temperature parageneses showed them to be uncontaminated by any 7-Å phase.

On Figure 1, the ideal mica line has the equation $H_2O = 2.50 - 1.50X$, where X is the molar sum K + Na +

[1] A copy of Appendices 1 and 2 may be ordered as Document AM-91-473 from the Business Office, Mineralogical Society of America, 1130 Seventeenth Street NW, Suite 330, Washington, DC 20036, U.S.A. Please remit $5.00 in advance for the microfiche.

Rb + Cs + NH_4 + Ca + Sr + Ba + 0.33(F + Cl). Least-squares linear regression for the data array yields H_2O = 2.365(0.154) − 1.394(0.145)X, with a correlation coefficient $r = -0.893$. Parenthesized values in this fit equation are the 95% confidence limits (1.96σ) on the ordinate intercept and slope. Use of the simple least-squares regression procedure is justified in the following section on error assessment. The regression fit is shown on Figure 1 as a dashed line, whereas the molecular component mixing lines are plotted as solid lines. The correlation shows that 80% (= 100 r^2) of the variation in measured $H_2O(+)$ content of white micas is associable with halogen-OH exchange and with exchange of vacancies and H_2O and H_3O^+ for sodium cesium alkalis and calcium barium alkaline earths in interlayer sites; the other 20% of the variance of $H_2O(+)$ is scatter having causes not addressed by the abscissa variable. With reference to forthcoming variance analysis, it is apparent that any model for white mica stoichiometry that considers only these three mechanisms for structurally incorporating H_2O cannot possibly account for more than 80% of the variance in reported $H_2O(+)$. If any subset of the three exchange operators (mixing lines) identified in Figure 1 can account for all 80% of the variance associable with this x-y correlation, then the remaining operator(s) may be identified as inoperative. The following two sections of the paper aim to weigh the principal components of the variance in Figure 1.

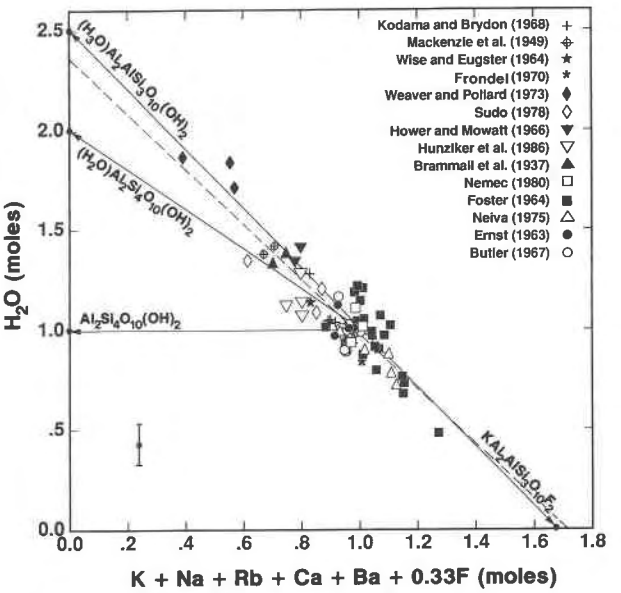

Fig. 1. Variation of the molar proportion of structurally bound H_2O, $H_2O(+)$, with the sum of the molar proportions of large alkali and alkaline earth cations occupying interlayer sites plus ⅓ of the halogens that substitute for OH. The solid lines are mixing lines or substitutional composition vectors among the identified molecular components. The dashed line is a least-squares fit. The error cross represents average bounds of probable error as defined in the text.

Models for stoichiometry of H_2O-rich micas

The basic approach is to calculate the stoichiometric proportions of tetrahedral, octahedral, and interlayer cations appropriate to balance the negative charge (−22) contributed by $O_{10}(OH,F,Cl)_2$ in the standard formula, utilizing the analyzed weight percent oxides except $H_2O(+)$, which is to be predicted according to three alternative models:

Model 1. All interlayer sites not occupied by alkali and alkaline earth cations are occupied by neutral H_2O molecules associable with a hydropyrophyllite molecular component in which H_2O molecules occupy well defined crystallographic sites rather than undefined positions hydrating interlayer cations, as in expandable clays and clay mixtures.

Model 2. A deficit in the interlayer charge contributed by alkali and alkaline earth cations is assumed to be satisfied by hydronium ions. After H_3O^+ balances the interlayer charge against that of the 2:1 layer, any interlayer sites not yet occupied by K, Na, Rb, Cs, Ca, Sr, Ba, or H_3O^+ are considered empty and associable with a pyrophyllite molecular component. This model, incorporating a hydronium-muscovite component, is essentially that proposed by Brown and Norrish (1952). It considers that the dashed regression trend on Figure 1 is a combination of a dominant vector toward hydronium muscovite at x,y = 0,2.5 and a minor component toward pyrophyllite at 0, 1.0.

Model 3. Like model 2, except that interlayer sites considered vacant in model 2 are considered in model 3 to be occupied by neutral H_2O molecules; i.e., the interlayer may contain both H_2O and H_3O^+, associable with hydropyrophyllite and hydromica components, respectively. There is no pyrophyllite component (cf. Fig. 1).

In model 1, the number of cations (other than H) is normalized to yield a total charge of 22. Cation proportions, n_i, are assigned to structural sites as follows: tetrahedral $n^{[4]}\text{Al} = 4 - n\text{Si}$; the remaining Al and all transition elements and Zn, Mg, and Li are assigned to octahedral sites; all K, Na, Rb, Cs, Ca, Sr, and Ba are considered to occupy interlayer sites. The number of OH groups is $n\text{OH} = 2 - n\text{F} - n\text{Cl}$. If the sum of interlayer cations (*INTCAT*) is ≤ 1, then the number of interlayer H_2O molecules is $n\text{H}_2\text{O} = 1 - INTCAT$. (A computer program in Basic is included as Appendix 2 for calculation of mica formulas from microprobe or other analyses lacking $H_2O(+)$ determinations. The descriptive acronym variables used in the program are also used here for continuity and clarity. The acronym variables are italicized.) In model 1, neutral H_2O molecules are considered to occupy all interlayer sites that are not occupied by cations. The calculated stoichiometric content of total H_2O as OH^- and interlayer H_2O^0 may be calculated by the proportionality relation utilizing molecular weights of H_2O and silica:

$$\text{wt\% } H_2O/[18.0153(n\text{H}_2\text{O} + 0.5n\text{OH})] = \text{wt\% } SiO_2/60.084n\text{Si}. \quad (1)$$

In model 2, interlayer sites that are not occupied by alkali and alkaline earth cations may be vacant or occu-

TABLE 1. Molecular components of white micas utilized in calculation of structural formulas

Formula	Label
$KAl_2AlSi_3O_{10}(OH,F)_2$	MUSC
$KFe^{3+}_2AlSi_3O_{10}(OH)_2$	FEMUS
$(Rb,Cs)Al_2AlSi_3O_{10}(OH)_2$	RBMUS
$NaAl_2AlSi_3O_{10}(OH)_2$	PARA
$CaAl_2Al_2Si_2O_{10}(OH)_2$	MARG
$BaAl_2Al_2Si_2O_{10}(OH)_2$	BAM
$KLi_2AlSi_4O_{10}(F,OH)_2$	PLITH
$K(Mg,Fe^{2+})TiAlSi_2O_{10}(OH)_2$	TIM
$K(Mg,Fe^{2+})CrSi_4O_{10}(OH)_2$	CRCLD
$K(Mg,Mn,Zn,Fe^{2+})AlSi_4O_{10}(OH)_2$	ALCLD
$K(Mg,Fe^{2+})Fe^{3+}Si_4O_{10}(OH)_2$	FECLD
$\square Al_2Si_4O_{10}(OH)_2$ (model 2 only)	IVAC
$(H_2O)Al_2Si_4O_{10}(OH)_2$ (models 1 and 3)	PYRO
$(H_3O)Al_2AlSi_3O_{10}(OH)_2$ (models 2 and 3)	HYD

Note: The component labels are utilized in output of the computer program in Appendix 2.

pied by hydronium ions. An iterative procedure is employed to estimate the number of hydronium ions by charge balance, given the starting assumption that the only trioctahedral component in the mica solid solution is polylithionite, $KAlLi_2Si_4O_{10}(OH)_2$. Therefore, in the standard formula the octahedral and tetrahedral cations sum as $OCTTET = 6 + 0.5n\text{Li}$, and the proportion of interlayer cations $INTCAT$ is normalized to that value of $OCTTET$. An initial estimate of the number of interlayer vacancies is made by stoichiometric balance on Si, with the assumption that the white mica solid solution consists of the molecular components listed in Table 1; i.e., the number of Si atoms is 3 plus the mole fractions of tetrasilicic celadonite and pyrophyllite components, minus the mole fractions of bisilicic Ba and Ca components, etc. Rearrangement gives the number of interlayer vacancies, $IVAC$ (= pyrophyllite mole fraction), relative to the number of other atoms in the standard formula as

$$IVAC = n\text{Si} + n\text{Ba} + n\text{Ca} + n\text{Ti} - n\text{Fe}^{2+} - n\text{Mg} - n\text{Mn} - n\text{Zn} - n\text{Li} - 3. \quad (2)$$

For $IVAC \geq 0$, the estimated number of hydroniums is

$$n\text{H}_3\text{O} = 1 - INTCAT - IVAC. \quad (3)$$

With $n\text{H}_3\text{O} \geq 0$, the total ionic charge is then calculated. If the total cationic charge (excluding H in OH groups) differs from 22 by more than 0.005 (or other preselected value of the convergence tolerance), then the total number of $OCTTET + INTCAT$ atoms is incremented or decremented as appropriate for convergence on the desired total charge. In each iteration, the difference from the desired charge is divided by the average charge per $OCTTET$ cation to obtain an increment, I, in number of $OCTTET$ cations, and I is used to obtain a renormalization factor, K, for all cations: $K = (OCTTET - \text{I})/OCTTET$, where I may be positive or negative. In each iteration a new K is multiplied by the old nSi, nAl, nCa, etc., and the number of interlayer vacancies and hydroniums is recalculated according to Equations 1 and 2. The calculation normally converges on the charge balance with the desired precision

TABLE 2. Comparison of structural formulas calculated according to models 1, 2, and 3 for two hydrothermal micas

	SER* wt%	Model 1	Model 2	Model 3	TOB** wt%	Model 1	Model 2	Model 3
		Atomic				Atomic		
SiO_2	48.39	3.2117	3.1890	3.1890	48.40	3.1753	3.1440	3.1440
TiO_2	0.11	0.0055	0.0055	0.0055	0.02	0.0010	0.0010	0.0010
Al_2O_3	34.64	2.7097	2.6905	2.6905	36.27	2.8045	2.7768	2.7768
Fe_2O_3	1.15	0.0574	0.0570	0.0570	0.00	—	—	—
FeO	0.27	0.0150	0.0149	0.0149	0.51	0.0282	0.0279	0.0279
MnO	0.00	—	—	—	N.A.	—	—	—
MgO	0.44	0.0435	0.0432	0.0432	0.52	0.0509	0.0504	0.0504
CaO	0.26	0.0114	0.0113	0.0113	0.00	—	—	—
Na_2O	0.22	0.0283	0.0281	0.0281	0.04	0.0050	0.0050	0.0050
K_2O	7.82	0.6621	0.6574	0.6574	2.30	0.1925	0.1906	0.1906
$(NH_4)_2O$	N.A.	—	—	—	3.51	0.5313	0.5261	0.5261
Li_2O	trace	—	—	—	N.A.	—	—	—
F	0.06	0.0126	0.0125	0.0125	N.A.	—	—	—
$H_2O(+)^{105}$	6.07				6.40			
$H_2O(-)^{105}$	0.44				1.97			
less O = F	0.03				—			
Sum	99.90				99.94			
OCTTET		6.0427	6.0000	6.0000		6.0598	6.0000	6.0000
INTCAT		0.7018	0.6968	0.6968		0.7288	0.7217	0.7217
IVAC		—	0.1476	—		—	0.0668	—
$n\text{H}_2\text{O}^0$		0.2982	—	0.1476		0.2712	—	0.0668
$n\text{H}_3\text{O}^+$		—	0.1556	0.1556		—	0.2115	0.2115
$n\text{OH}^-$		1.9874	1.9875	1.9875		2.0000	2.0000	2.0000
wt% $\Sigma\ H_2O(+)_{calc}$		5.84	5.58	6.25		5.81	6.08	6.39
Σ charge		22.0004	22.0000	22.0000		22.0057	22.0000	22.0000

Note: N.A. = not analyzed.

* SER is a soft, pale prase-green, waxlike hydrothermal sericite from veinlets containing quartz, base-metal sulfides, and Au at Ogofau, Carmarthenshire, southern Wales, reported by Brammall et al. (1937). X-ray diffraction showed trace apatite impurity, subtracted from the analysis above.

** TOB is a very fine-grained tobelite from Tobe, Ehime Prefecture, Japan, reported by Higashi (1982). Fe^{2+}/Fe^{3+} not analyzed, but the high NH_4 content and association with graphite require that $Fe_{tot} \simeq Fe^{2+}$, with negligible uncertainty. X-ray diffraction showed, by the quantitative method of standard additions, the presence of 2.5 wt% quartz, subtracted from the analysis, which was then renormalized to the original total.

in two cycles. For model 2, the total H_2O content as H_3O^+ and OH^- is calculated as

$$\text{wt\% } H_2O = 18.0153(1.5nH_3O + 0.5nOH) \cdot(\text{wt\% } SiO_2/60.084nSi). \quad (4)$$

In model 3, the procedure of model 2 is modified only by occupying the calculated number of interlayer vacancies with neutral H_2O molecules. The stoichiometric total H_2O content then becomes the sum of contributions by OH^-, H_3O^+, and H_2O^0 by combining Equations 1 and 4.

Table 2 provides examples of structural formulas and total H_2O contents calculated according to models 1, 2, and 3. The tobelite sample was not included in the data set statistically analyzed because it is not a K-rich mica and because it lacks Fe^{2+} and Fe^{3+} determinations. (Criterion 3 was rigidly adhered to, even though there is no substantial uncertainty about the valence of Fe in this case.) It is included on Table 2 as an interesting example of a very hydronium-rich mica for which the chemical analysis closely approaches ideal stoichiometry. For both micas, note the relatively close correspondence of model 3's calculated total H_2O with measured $H_2O(+)$. Note also the *OCTTET* excess that is a persistent feature of model 1 and of the heretofore prevalent calculation convention that ignores hydronium in micas and consequently finds a widely reported but spurious correlation between an apparent deficiency of interlayer cations and an apparent excess of octahedral cations in the charge-balanced formula.

Comparison of measured $H_2O(+)$ with model predictions

Figure 2A compares measured $H_2O(+)$ with the calculated H_2O content according to model 1, which has interlayer H_2O but no hydronium. The heavy line having unit slope would represent perfect correspondence of measured $H_2O(+)$ and calculated structural H_2O contents. Least-squares linear regression of the 72 points in the array

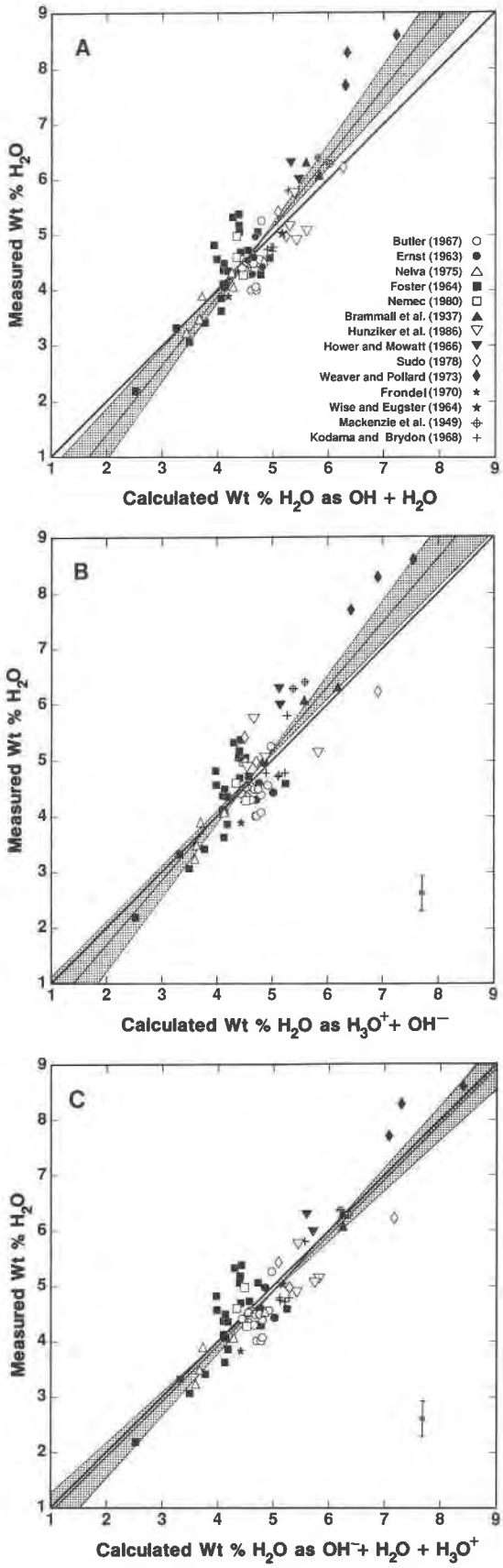

→

Fig. 2. (**A**) Measured content of bound H_2O, $H_2O(+)$, compared with calculated total H_2O content as predicted by model 1. The complete analyses are listed in Appendix 1. The stippled wedges representing the 95% confidence interval about the least-squares regression fit (thin line) do not enclose the heavy line of unit slope that represents 1:1 correspondence of measured and calculated water content. (**B**) Comparison of measured $H_2O(+)$ with the total H_2O content as predicted by model 2. The stippled 95% confidence interval about the least-squares fit (thin line) does not enclose the heavy line of unit slope that signifies 1:1 accord of calculated and measured values. (**C**) Comparison of measured H_2O contents with total H_2O as predicted by model 3. The least-squares fit (thin line) is nearly coincident with the heavy line representing perfect agreement of the model values with measured values, which demonstrates excellent accord between model 3 and the observations. The error cross represents bounds of probable error (defined and derived in the text) for each data point.

yields the fit equation $\%H_2O_{meas} = 1.2406\ H_2O_{calc} - 1.036\%$ with a correlation coefficient $r = 0.889$. The standard error of the slope is $\sigma_s = 0.0675$ evaluated according to Till (1974, p. 102, assuming that errors in the analytical data are normally distributed), which yields the stippled wedges showing the 95% ($1.96\sigma_s$) confidence interval about the slope. The slope rotates through standard-error wedges having bow-tie symmetry about the pivot point or centroid corresponding to the mean (4.77% H_2O_{meas}). The bow-tie error bounds on the slope are not to be confused with similar-looking and more familiar, hyperbola-enclosed, standard-error bounds on values of the dependent variable, H_2O_{meas}. The treatment of H_2O_{meas} as a dependent variable in the regression will be justified in the following discussion of errors. The line of unit slope lies outside the 95% confidence interval about the regression slope in Figure 2A, so model 1 can be rejected as inappropriate or inadequate to explain the observed pattern of variation of H_2O contents of the micas. In fact, the slope of 1.2406 lies $3.564\sigma_s$ from the 1.1 agreement line, so more than 99.9% of the probability distribution for the model 1 slope lies at values >1.

In Figure 2B, the same measured $H_2O(+)$ values are plotted against structural H_2O contents as predicted by model 2, which makes provision for interlayer hydronium ions but not neutral H_2O molecules. The mean of the measured $H_2O(+)$ values is 4.77 wt%, whereas the mean of calculated structural H_2O content is 4.68 wt%. Least-squares linear regression yields the equation $\%H_2O_{meas} = 1.1496\ H_2O_{calc} - 0.608\%$, with $r = 0.863$ and $\sigma_s = 0.0689$. Because this value of the slope is nearer to unity, it is apparent that model 2 provides a better description of the data than model 1; however, the stippled 95% confidence interval about the fit slope fails to include the line of unit slope, so model 2 also fails to provide an adequate description of factors controlling mica H_2O content. In the normal probability distribution for the model 2 slope, 98.5% of it lies at values >1.

In both models 1 and 2, the calculated structural H_2O content is usually less than the measured $H_2O(+)$. It seems reasonable to expect that (unlike pyrophyllite in which neighboring 2:1 layers are translated so as to distort, shrink, and virtually eliminate mica-type interlayer sites) in micas containing a deficit of interlayer cations resulting from the presence of a pyrophyllite-like, tetrasilicic molecular component, the sites that are inferred to be vacant in model 2 are large open sites that may readily be occupied by neutral atoms (e.g., Ar) or molecules (e.g, H_2O or H_4C) comparable in size to the simple K^+ ion or the polyatomic ions H_4N^+ and H_3O^+. Pursuing this intuition, interlayer sites vacant in model 2 are occupied by neutral H_2O molecules in model 3.

Total structural H_2O contents predicted by model 3 are plotted against measured $H_2O(+)$ in Figure 2C. Least-squares linear regression of the 72 analyses yields the equation $\%H_2O_{meas} = 1.0081\ H_2O_{calc} - 0.103\%$, with $r = 0.902$, a standard error of the slope $\sigma_s = 0.0514$, and standard error of the intercept $\sigma_i = 0.252$. The discrepancy between the mean $H_2O(+)_{meas}$ (4.77 wt%) and mean H_2O_{calc} (4.83 wt%) is 30% smaller than the discrepancy for models 1 and 2. Thus, model 3 provides a modest decrease in data dispersion and a dramatic improvement in model fit (nearly perfect coincidence with the 1:1 line; the separation between the lines is exaggerated for clarity in Fig. 2C).

Error analysis

This section evaluates the relative magnitudes of standard error bars of the ordinate and abscissa variables in Figures 2A–2C, as needed to justify the regression procedure selected from among the alternatives of unweighted least-squares regression of x on y or y on x, reduced major axis regression, or datum-individualized differential weighting schemes. The appropriate choice established the statistical criteria for adopting or rejecting mica composition models 1, 2, or 3.

Predicted stoichiometric H_2O

The imprecision of the abscissa variable, estimates of the wt% H_2O structurally bound in OH and interlayer sites according to stoichiometries described by models 1, 2, or 3, results from the cumulative analytical uncertainty in wt% SiO_2, Al_2O_3, K_2O, Na_2O, etc. propagated through the stoichiometric model:

$$\sigma^2_{H_2O(calc)} = \sigma^2_{SiO_2}(\partial W_{H_2O}/\partial W_{SiO_2})^2 + \sigma^2_{Al_2O_3}(\partial W_{H_2O}/\partial W_{Al_2O_3})^2 + \sigma^2_{K_2O}(\partial W_{H_2O}/\partial W_{K_2O})^2 + \ldots \quad (5)$$

in which W_i is the weight percent of oxide constituent i, and the variances σ^2 refer to weight percent also. Evaluating variances of wt% SiO_2 and other oxide constituents is not straightforward because the Appendix 1 data set is a compilation of work by many analysts using a variety of classical wet-chemical methods (chiefly gravimetric, colorimetric, and volumetric). None of the published sources numerically assesses analytical errors, so these must be estimated from statistical properties of the data collection as a whole. Average analytical uncertainties of individual major oxide constituents can be inferred from the variance of their summations:

$$\sigma^2_\Sigma = \sigma^2_{SiO_2} + \sigma^2_{Al_2O_3} + \sigma^2_{K_2O} + \sigma^2_{H_2O} + \ldots = \sum_i (k\epsilon W_i)^2 \quad (6)$$

in which ϵ is the fractional error in W_i and k is a weighting factor. The following analysis proceeds by evaluating σ^2_Σ for the Appendix 1 data set and then solving Equation 6 for ϵ at selected values of k and W_i.

In order for the variance of analysis totals in Appendix 1 to represent accurately the typical analytical uncertainties in individual oxide constituents, it must be established that the screening criteria for selection have not unduly biased the sample—viz., has the exclusion of mica analyses having totals $<99.5\%$ and $>100.5\%$ produced a histogram of analysis totals that represents a bar 99.5–100.5%

wide corresponding to the central slice of a much more diffuse distribution in a parent population of imprecise mica analyses? Or does the histogram of analysis sums represent an essentially complete frequency distribution of a population of truly superior, precise analyses?

A histogram of the 72 analysis totals, partitioned in intervals of 0.1 wt%, shows a somewhat skewed distribution with a high mean, resulting primarily from systematic error in the largest group of analyses from a single analyst—the set of 13 analyses by Butler (1967), which are as precise ($\sigma_\Sigma = 0.24$ wt%) as the rest of the analyses in Appendix 1 ($\sigma_\Sigma = 0.23$%), but Butler's subset has a high mean of 100.19 wt%. If Butler's set is corrected for systematic error by subtracting 0.19 wt% from each analysis sum, the resulting histogram for all 72 analyses is a symmetric bell-shaped distribution with a mean of 99.99_3 wt% and standard deviation $\sigma_\Sigma = 0.23_3$ wt%. The range 99.5–100.5 wt% spans $2.15\sigma_\Sigma$ on either side of the mean, which corresponds to 97% of the area under a normal probability curve. A χ^2 comparison with a normal probability distribution divided into quartiles at $X_\Sigma - 0.67\sigma_\Sigma$, X_Σ, and $X_\Sigma + 0.67\sigma_\Sigma$ yields a value of $\chi^2 = 0.111$, signifying negligible deviation of the data set in Appendix 1 from the complete, normal frequency distribution of a population of truly precise analyses (not a severely truncated central slice out of a population of imprecise analyses). Therefore, the value $\sigma_\Sigma = 0.23$ wt% may be used in Equation 6.

Lacking the information necessary for individualized treatment, it is reasonable to assume that error in analysis sums is derived chiefly from errors in major oxide constituents and that, in a first approximation , the relative error factor, ϵ, does not differ appreciably among major oxide constituents. It will be assumed that the weighting factor k is unity for all oxides except $H_2O(+)$. For a variety of reasons listed in the next section, the relative error in determinations of structurally bound H_2O is generally about an order of magnitude larger than error in other major constituents, i.e., for $H_2O(+)$, $k \simeq 10$. With these simplifying assumptions regarding error factors ϵ and k, the standard error in major constituents of a typical muscovite sample can be represented by that of end-member muscovite, which has 45.255 wt% SiO_2, 38.397 wt% Al_2O_3, 11.825 wt% K_2O, and 4.523 wt% H_2O. Substitution of these values into Equation 6 yields $\epsilon = 0.0031$, $\sigma_{SiO_2} = 0.14$ wt%, $\sigma_{Al_2O_3} = 0.12$ wt%, $\sigma_{K_2O} = 0.04$ wt%, and 95% confidence intervals on determinations of major constituents of ideal muscovite as follows: 44.97–45.54 wt% SiO_2, 38.16–38.64 wt% Al_2O_3, and 11.75–11.90 wt% K_2O. These representative σ_i values can be substituted into Equation 5.

The partial derivatives in Equation 5 may be evaluated empirically as finite-difference derivatives using an arbitrary but representative hydronium-bearing muscovite composition, $K_{0.9}(H_3O)_{0.1}Al_3Si_3O_{10}(OH)_2$. Its contents of SiO_2 (45.484 wt%), Al_2O_3 (38.592 wt%), and K_2O (10.696 wt%) were individually and sequentially perturbed by $\pm 1\sigma_i$ as given above, and the wt% H_2O in the perturbed composition was calculated according to stoichiometric model 3, giving $\partial W_{H_2O}/\partial W_{SiO_2} = 0.1075$, $\partial W_{H_2O}/\partial W_{Al_2O_3} = 0.1899$, and $\partial W_{H_2O}/\partial W_{K_2O} = 0.5682$. Substituting these into Equation 5 gives an estimated typical value of $\sigma_{H_2O(calc)} = 0.03_4$ wt%. The horizontal error bar on Figure 2 corresponds to the probable error $PE = 0.6745\sigma_{H_2O} = \pm 0.02$ wt% H_2O. This PE bound corresponds to the 50th percentile on the cumulative frequency curve of normally distributed error (Bevington, 1969, p. 46, 94). This small imprecision in the calculated stoichiometric proportion of H_2O that is the consequence of propagated imprecision in analyses of SiO_2, Al_2O_3, etc. is to be compared with errors in direct measurements of H_2O content, which are assessed below.

Uncertainties in measured structural H_2O

Nearly 90% of the H_2O determinations in the data set in Appendix 1 were conducted since 1930 by the Penfield method or a minor variant of it (Peck, 1964), in which a weighed portion of the sample is loaded into a very long-necked, stoppered bulb flask that is held horizontally while heating the bulb end and its charge to "red heat" (usually over a flame) to liberate the volatiles; the H_2O fraction is then condensed within the stoppered neck cooled by a wet towel. The bulb and its dehydrated charge are then separated from the flask by heating the join to fuse the glass, which can be pulled apart to leave the H_2O sealed inside the stoppered tube. The tube and its contained H_2O are weighed, then dried and reweighed to obtain the H_2O mass by difference.

The wt% $H_2O(-)$ is determined on a separate aliquot of the sample as the weight loss before and after drying it several hours in an oven at 105 ± 5 °C. The wt% $H_2O(+)$ is obtained as the difference between $H_2O(-)$ and total H_2O determined by the Penfield method.

Weighing errors. For whole-rock analyses in which plenty of sample is available, the Penfield procedure usually uses 1 g of sample. With a notch-and-chain-type analytical balance in common use before 1970, customary weighing precision is around 0.1–0.2 mg, and the stated precision of total H_2O determinations on large samples by experienced, careful analysts is around 0.01–0.02 wt% (Peck, 1964). However, it is laborious and difficult to obtain large amounts of high-purity separates of fine-grained micas by a combination of heavy liquid separation, sedimentation, magnetic separation, and hand picking; furthermore, the mica separate must be split into several aliquots for separate treatment by various wet-chemical analytical procedures. Because of supply constraints, the mass of mica used for thermogravimetric measurement of H_2O is commonly 100–200 mg, so the analytical precision on such small samples is around $0.X$ wt%, in contrast to $0.0X$ wt% on gram-size samples.

The $H_2O(-)$ determination is prone to error because fine-grained sericite or illite and finely ground muscovite are strongly hygroscopic and may rehydrate quickly after removal from the drying oven, even as the sample is being weighed. Upon subtraction from total H_2O, that error in $H_2O(-)$ propagates to $H_2O(+)$.

Several analysts reported as $H_2O(+)$ the weight loss

during DTGA as the mica aliquot was heated from 105 ± 5 °C to ~1000 °C in air. That procedure is subject to error because of oxidation of FeO to Fe_2O_3. Many metamorphic and igneous muscovite samples in Appendix 1 have 1–3 wt% FeO. Upon complete oxidation, 1 wt% FeO becomes 1.1 wt% Fe_2O_3, which translates to errors on the order of 0.X wt% in reported $H_2O(+)$ if no correction is applied. In virtually all sources of data in Appendix 1, the description of analytical procedures is sketchy and does not indicate whether precautions or corrections were used.

Fluid inclusions. The Penfeld and DTGA determinations of $H_2O(+)$ cannot distinguish H_2O liberated by decrepitated fluid inclusions from H_2O in crystallographic sites. There seems to be no published information on the abundance of aqueous fluid inclusions in micas, although silicate melt and CO_2 inclusions in mica are described by Roedder (1984, p. 481, 516). Presumably micas may trap submicroscopic aqueous inclusions in abundances similar to their proportion in associated quartz, feldspars, topaz, beryl, sulfides, etc., which commonly attains 0.0X to 0.X wt% (Roedder, 1984, p. 111; Aines and Rossman, 1984; Hofmeister and Rossman, 1985).

Inconsistent and inappropriate drying temperatures. DTGA studies on sericite and illite commonly report continuous weight loss over the 50–200 °C interval, with no break to distinguish adsorbed moisture from H_2O bound in crystallographic sites (MacKenzie et al., 1949; Kodama and Brydon, 1968; Norrish and Pickering, 1983; Newman and Brown, 1987). That behavior has generated uncertainty as to what drying temperature is an appropriate boundary between $H_2O(-)$ and $H_2O(+)$. Many analyses in Appendix I, especially the older ones, used drying temperatures of 105 °C or occasionally even 100 °C; a number of the more recent ones used 110 °C; many authors fail to specify their boundary between $H_2O(-)$ and $H_2O(+)$. Micas from hydrothermal and sedimentary parageneses commonly report 1–3 wt% $H_2O(-)$; the difference between an accurate measurement as $H_2O(+)^{105°C}$ and as $H_2O(+)^{110°C}$ may amount to 0.1 wt% or more. Therefore, inconsistency among analysts in choice of drying temperature may contribute further scatter on Figure 2, amounting to ca. 0.1 wt% $H_2O(+)$.

Conclusion and application to linear regression

The uncertainties in measurements of structurally bound H_2O that are the result of analytical error, uncertainty in what drying temperature is appropriate to discriminate hygroscopic moisture from structurally bound H_2O, and inconsistency among analysts in choice of drying temperature collectively contribute imprecision and inaccuracy, probably amounting to several tenths of a weight percent to estimates of structurally bound H_2O as represented by measurements of $H_2O(+)$.

The imprecision of analyses of wt% SiO_2, Al_2O_3, K_2O, Na_2O, etc. propagates through stoichiometric models 1, 2, and 3 to yield an imprecision $\sigma_{H_2O(calc)} \simeq 0.03$ wt%, which is about an order of magnitude smaller than uncertanties in direct measurements of structurally incorporated H_2O. These considerations justify the treatment of the ordinate variable in Figures 1 and 2 as a dependent variable containing virtually all the uncertainty that is expressed as scatter about the regression trend. A differential weighting regression procedure, more elaborate than the simple least-squares regression in Figures 1 and 2, does not appear to be warranted by the available information on uncertainties.

In Figure 2C, the standard deviation of measured wt% $H_2O(+)$ about the regression line is $s_w = 0.46$ wt% (following Till, 1974, p. 46) and is similar in the other two diagrams. The vertical error bars shown on Figures 2A–2C represent the probable error, PE = 0.6745 $s_w = \pm 0.31$ wt% H_2O.

Conclusions from model tests

Measurements of $H_2O(+)$ tend to be about 0.06 wt% short of values predicted by model 3 [the difference in the means of calculated and measured $H_2O(+)$], and the regression intercept of −0.103 wt% might be suspected to constitute further evidence for a modest proportion of unhydrated interlayer vacancies throughout the data set. However, it may be noted that the apparent deficit of $H_2O(+)_{meas}$ is smaller (<0.05 wt%) near the H_2O-rich end of the data array than near the H_2O-poor end of the array (>0.09 wt%), which suggests that the source of the discrepancy is not in interlayer site occupancies but rather in OH site occupancies. Has neglect of a significant exchange operator, such as O^{2-} for OH^-, produced a systematic defect in the stoichiometric model? The standard error of the model 3 regression intercept, $\sigma_i = 0.25$ wt%, embodies both the uncertainty in the regression slope and the uncertainty in location of the pivot (the mean) through which it rotates. Given an infinite population of micas having on average the properties of model 3 but normally distributed variance in measured $H_2O(+)$ of the magnitude present on Figure 1, there is a 67% probability that a random sample of 72 micas would yield a regression intercept deviating from zero by ≥0.103 wt% $H_2O(+)$ (i.e., 0.41σ_i). The model 3 regression slope of 1.008 differs from the ideal unit slope by 0.158σ_s (in which the standard error of the slope $\sigma_s = 0.051$). The interval ±0.158σ_s about the fit slope encloses 13% of its normal probability distribution. That is, even if model 3 were a perfect description of the mica population, the analytical (and sampling) uncertainties are of a magnitude such that there is an 87% probability of obtaining a regression slope value deviating from unity by ≥0.008. Therefore, the difference of the regression intercept value from zero and the difference of the regression slope from unity cannot be construed as statistically significant evidence for another unconsidered stoichiometric substitution vector or a pervasive defect in the chemical analyses that produces systematic deviation of calculated from measured $H_2O(+)$.

From the value $r^2 = 0.81$ for Figure 2C, it is apparent that crystallochemical model 3 explains 81% of the variance of the measurements of $H_2O(+)$. From the observation that the variance of the array in Figure 1 (which

plots only measured, not inferred, parameters but embodies all the substitution operators considered by model 3) is $r^2 = 0.80$ (identical within roundoff uncertainty), it is evident that model 3 accounts for all the systematic variation (correlation) that is present in Figure 1. It succeeds in doing so without invoking any statistically significant role for interlayer vacancies. This conclusion and the linear regression intercept in Figure 1 indicate that, on average, the hydromica substitution $(H_3O)K_{-1}$ accounts for 73% of interlayer H_2O in the sample group, whereas the hydropyrophyllite substitution $H_2OSi(KAl)_{-1}$ accounts for only 27% of the interlayer H_2O in the average muscovite.

In summary, within the resolution of the measurements, the crystal-chemical model that considers all interlayer sites to be occupied by conventional alkali and alkaline earth cations, hydronium ions, and H_2O molecules explains all the crystal-chemical systematic variation in measurements of white mica H_2O content. The remaining 20% of the variance in $H_2O(+)$ that is uncorrelated with the substitution operators considered by Figure 1 and model 3 is largely attributable to random analytical errors and uncertainties itemized in the preceding section.

Hydration energies of interlayer vacancies

Stoichiometries calculated according to models 2 and 3 are identical in proportions of all ions, including hydronium, but model 2's interlayer vacancies are completely hydrated in model 3. The regression trend for model 2 (Fig. 2B) indicates a 98.5% probability that some or all its "vacancies" are occupied by neutral H_2O molecules. The regression statistics for model 3 (Fig. 2C) indicate that the most probable situation is that >95% of them are hydrated, which implies a strong thermodynamic drive for the reaction

$$\square Al_2Si_4O_{10}(OH)_2 + H_2O = (H_2O)Al_2Si_4O_{10}(OH)_2. \quad (7)$$

Taking the standard states to be pure liquid H_2O and pure solids at the temperature and pressure of interest and taking both mica components to have the same muscovite crystal structure, the standard Gibbs energy of Equilibrium 7 is given by $\Delta_r G^0_7 = -RT \ln(a_{H_2O}/a_{\square})_{mica} + RT \ln a_{H_2O,fluid}$. If $a_{H_2O,fluid} \simeq 1$ and if $(a_{H_2O}/a_{\square})_{mica} > 0.99/0.01$ in interlayer sites, then at the typical analytical drying temperature of 105 °C, $\Delta_r G^0_7$ would be more negative than −14.4 kJ/mol.

That hydration energy is broadly comparable to the contribution of molecular H_2O to the stability of zeolites and montmorillonites. For example, $\Delta_r G^0 = -25.4$ kJ/mol at 105 °C and 1 bar for hydration of dehydrated analcime, $NaAlSi_2O_6 + H_2O_{liq} = NaAlSi_2O_6 \cdot H_2O$ (Helgeson et al., 1978), which corresponds to $a_{H_2O}/a_{\square} = 0.9997/0.0003$ in analcime if $a_{H_2O,liq} = 1$. Keren and Shainberg (1975) calorimetrically determined $\Delta_r H^0 = -13.8$ kJ/mol H_2O at 25 °C for adsorption of 1–4 mol of H_2O per mole of Ca^{2+} ions in the interlayer region of calcium beidellite. If the molar entropy of that H_2O hydrating interlayer Ca^{2+} ions is assumed to be similar to the entropy of zeolitic H_2O (59 J/mol·K H_2O in analcime; Helgeson et al., 1978), then $\Delta_r S^0 \simeq 10.9$ J/mol·K and $\Delta_r G^0 \simeq -10.6$ kJ/mol H_2O for adsorption of a molecular H_2O monolayer in the interlayer region of calcium beidellite. That is likely to represent a smaller binding energy that that of crystallographically sited H_2O in micas. Considering a representative single-phase illite such as that described by MacKenzie et al. (1949; analysis 55 in Appendix 1 of this paper), which corresponds to the stoichiometry $[K_{0.652}Na_{0.017}(H_3O)_{0.124}(H_2O)_{0.207}]_{1.00}(Al_{1.709}Fe^3_{0.117}Fe^2_{0.033}Mg_{0.134}Ti_{0.007})_{2.00}(Si_{3.373}Al_{0.627})_{4.00}(OH)_{2.00} \cdot (H_2O)_{0.191}$, the neutral H_2O in interlayer crystallographic sites (not adsorbed on interlayer cations and grain surfaces) contributes around $\Delta_r G^0 \simeq (0.207)(-14.4) = -3$ kJ/mol or more (perhaps −5 kJ/mol) to that specimen's thermodynamic stability, compared to the equivalent mica with 0.207 interlayer vacancies per mole.

Interlayer H_2O variation with temperature

The 72 mica analyses in the data set (Appendix 1) have been divided according to apparent formation temperature into three groups on the basis of information provided by the original authors regarding the geologic context and paragenetic associations. The highest temperature category comprises muscovite and lepidolite from pegmatites and from gneisses and schists in the amphibolite or upper greenschist facies (above the biotite isograd in metapelites and metapsammites), corresponding to the approximate temperature range 450–700 °C. The intermediate-temperature group consists of sericites from hydrothermally altered rocks and from rocks regionally metamorphosed in the prehnite-pumpellyite, blueschist, and lower greenschist facies at temperatures around 150–450 °C. The low-temperature group consists of pedogenic and diagenetic white micas. This last group is small because few illite analyses passed the tests for mineralogic purity and the chemical screens previously described.

Figure 3 shows for these three temperature groups histograms of measured molar $H_2O(+) + 0.5(F + Cl)$, which has a value of 1.00 for an ideally stoichiometric muscovite, $KAl_2AlSi_3O_{10}(OH,F,Cl)_2$, but values greater than one for micas with interlayer hydronium and H_2O molecules. Figure 3 shows that the average H_2O content of the high-temperature micas does not differ significantly from the usual allotment to OH-halogen sites, although the individual samples show considerable variation. There is no apparent difference between micas from pegmatites and those from gneisses and schists with respect to interlayer H_2O content.

The hydrothermal and low-grade metamorphic micas show a broader range of H_2O content and a significantly higher mean content. In this group, interlayer H_2O averages about one-seventh of total structural H_2O, but a substantial fraction of the hydrothermal sericites have 20–30% of their total H_2O in interlayer sites.

The low-temperature sedimentary group in the lowest histogram has even more variation in structural H_2O and a substantially higher mean that corresponds to about one-

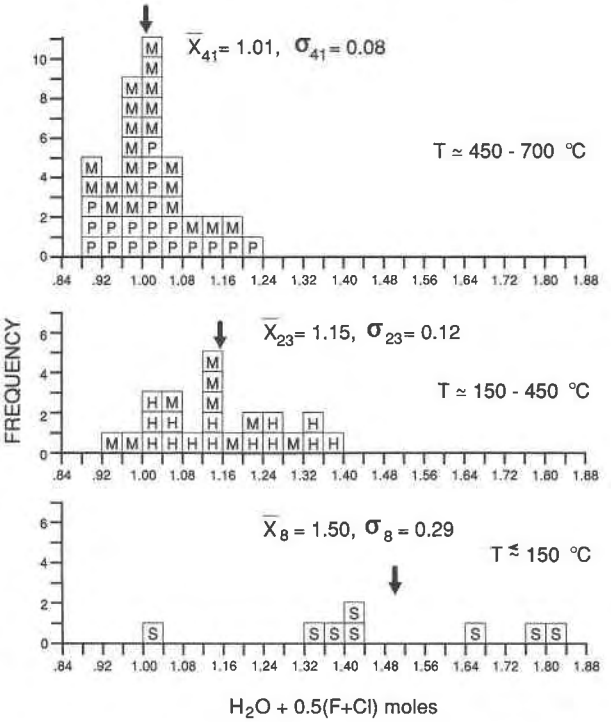

Fig. 3. Histograms of structurally bound H_2O plus halogen contents (molar) in potassic white micas from three temperature regimes. The upper diagram represents muscovite from granitic pegmatites (P) and metamorphic rocks (M) in the upper greenschist and amphibolite facies. The mean volatile content of 1.01 mol per formula unit in the 41 samples is marked by the arrow; σ is the standard deviation. The middle diagram represents sericites from hydrothermal (H) environments and metamorphic rocks (M) in the middle and lower greenschist, blueschist, prehnite-pumpellyite, and zeolite facies. The lower diagram represents illite from diagenetic and sedimentary (S) environments. All data are from the compilation in Appendix 1.

third of the total H_2O occupying interlayer sites but ranges up to nearly half.

With regard to the high $H_2O(+)$ contents of some sedimentary illites, it is interesting to note that Merino and Ransom (1982) analyzed by electron microprobe at very low-beam current (so as to get very small excitation volumes) individual illite flakes in clots associated with kaolinite and quartz cement in drill cores from sandstones undergoing diagenesis at ~100 °C, measured by downhole thermometry. A group of K-Na-Ca-poor grains having the high birefringence of mica yielded the analyses reproduced in Table 3 together with wt% H_2O and stoichiometries calculated according to model 3. These natural illite compositions are remarkably close to the join $(H_2O)Al_2Si_4O_{10}(OH)_2$-$(H_3O)Al_2AlSi_3O_{10}(OH)_2$. Of course, those analyses could not be included in the Appendix 1 data set because structural H_2O content was not directly measured.

Implications and applications

Thermodynamic stability of illite and hydronium muscovite

As a working definition, illite is here taken to be a fine-grained, single-phase, dioctahedral, potassic white mica that is related to muscovite by a substantially lower content of K + Na in interlayer sites and a ratio of Si:Al > 3:1 in tetrahedral sites (Środoń and Eberl, 1984). Fe and Mg are commonly present as subordinate but nonessential occupants of octahedral sites, ascribable to a tetrasilicic, dioctahedral, celadonite-like molecular component that is insufficient to account for illite's elevated Si:Al ratio.

It has been widely accepted for many years that much of illite's deficit of K and excess of Si relative to muscovite are attributable to solid solution toward pyrophyllite, $Al_2Si_4O_{10}(OH)_2$. Pursuing that notion, Lippmann (1982) noted that in metamorphic rocks, white micas show no appreciable miscibility with pyrophyllite up to their thermal stability limits, and from that he inferred that the paragonite-pyrophyllite and muscovite-pyrophyllite binary systems are characterized by a solvus having a critical point at higher temperature (and high P_{H_2O}) and limbs that diverge with decreasing temperature. The formation temperatures and inferred stoichiometries of natural illites project into the binary system $KAl_2AlSi_3O_{10}(OH)_2$-$Al_2Si_4O_{10}(OH)_2$ well within the low-temperature extrapolation of the metamorphic miscibility gap, which led Lippmann to conclude that illites are thermodynamically metastable with respect to a mechanical mixture of muscovite and pyrophyllite. Essene (1982, 1989) echoed Lippmann's conclusion that clay minerals in general are metastable.

Recently, Jiang et al. (1990) offered what they considered to be compelling corroboration of Lippmann's argument for illite metastability by describing thin laminae of nearly pure pyrophyllite interleaved with sheets of nearly pure muscovite in lamellar packets produced by thermal decomposition of illite during prograde metamorphism of pelites. Jiang et al. inferred that the initial illite had formed metastably within a muscovite-pyrophyllite solvus, and its decomposition into an equilibrium mixture of pyrophyllite and muscovite was kinetically prompted by thermal activation. Jiang et al. (1990) then proceeded to explore the extensive ramifications of illite metastability for sedimentary petrology.

The preceding arguments for metastability of illite are false because the molecular components of illite that are parental to pyrophyllite "exsolution" lamellae have neither the chemical composition nor the crystal structure of pyrophyllite. The development of pyrophyllite lamellae in muscovite can be better understood with reference to the origin of hemoilmenite lamellae in titanomagnetite than to the topology of the paragonite-muscovite join (a simple parabolic solvus in T-X space). Figure 4 shows the likely topology of phase relations along the binary joins $KAl_2AlSi_3O_{10}(OH)_2$-$(H_2O)Al_2Si_4O_{10}(OH)_2$ and $KAl_2AlSi_3O_{10}(OH_2)$-$(H_3O)Al_2AlSi_3O_{10}(OH)_2$. Phase boundaries rep-

TABLE 3. Electron microprobe analyses of alkali-poor illites

Sample	423/G1	423/F1	E67/B1(2)	E72/G1	E72/G2	E72/G3
			Wt%			
SiO_2	49.27	48.80	50.04	49.97	50.29	50.55
TiO_2	0.00	0.00	0.08	0.00	0.09	0.00
Al_2O_3	38.40	37.28	34.78	35.39	34.70	33.74
Fe_2O_3*	0.57	0.68	2.50	2.19	1.88	2.88
MnO	0.05	0.10	0.09	0.00	0.08	0.00
MgO	0.16	0.36	0.89	0.58	0.59	0.71
CaO	0.05	0.06	0.09	0.12	0.06	0.17
Na_2O	0.03	.05	0.00	0.28	0.00	0.01
K_2O	1.04	0.97	1.92	3.04	2.61	3.26
H_2O_{calc}	11.04	10.91	10.40	9.40	9.77	9.29
Sum	100.18	98.81	100.31	100.33	99.26	99.74
			Atomic			
Si	3.104	3.119	3.181	3.183	3.223	3.242
$^{[4]}Al$	0.896	0.881	0.819	0.817	0.777	0.758
$^{[6]}Al$	1.955	1.928	1.787	1.840	1.845	1.793
Ti	0.000	0.000	0.004	0.000	0.004	0.000
Fe	0.027	0.033	0.120	0.105	0.091	0.139
Mn	0.003	0.005	0.005	0.000	0.004	0.000
Mg	0.015	0.034	0.084	0.055	0.056	0.068
Ca	0.003	0.004	0.006	0.008	0.004	0.012
Na	0.004	0.006	0.000	0.035	0.000	0.001
K	0.084	0.079	0.156	0.247	0.213	0.267
$^{[12]}H_3O$	0.820	0.827	0.736	0.574	0.612	0.535
$^{[12]}H_2O$	0.090	0.084	0.102	0.136	0.171	0.186
OH	2.000	2.000	2.000	2.000	2.000	2.000

Note: All analyses by Merino and Ransom (1982). The illites are described as highly birefringent and occurring with kaolinite and quartz as diagenetic cement in sandstones at Kettleman North Dome, California. H_2O contents and stoichiometries calculated according to model 3.

* Fe^{3+}/Fe^{2+} not analyzed; Fe_{tot} as Fe_2O_3.

resenting thermal decomposition of hydropyrophyllite and hydronium muscovite molecular components are labeled a–d, keyed to reactions listed below.

Chemical reactions that occur in response to heating are driven by entropy production. The molar entropy of $(H_2O)Al_2Si_4O_{10}(OH)_2$ is unknown but may be estimated from the sum of the entropy contributions $\Delta_t S^0$ for the lattice transformation $Al_2Si_4O_{10}(OH)_{2,pyro} = \square Al_2Si_4O_{10}(OH)_{2,mica}$ and $\Delta_h S^0$ for the vacancy-hydration reaction $\square Al_2Si_4O_{10}(OH)_2 + H_2O_{liq} = (H_2O)Al_2Si_4O_{10}(OH)_2$; $S^0_{hydropyro} = \Delta_t S^0 + \Delta_h S^0 + S^0_{H_2O} + S^0_{pyro}$. With regard to the hydration reaction, the bonding environment of K^+ ions and H_2O molecules in micas resembles that in the crystal structure of analcite, pollucite, and high leucite. In micas, the six-member rings of aluminosilicate tetrahedra face each other directly across the interlayer region such that a pair of rings in opposing tetrahedral sheets creates the 12-fold coordination polyhedron to be occupied by alkalis, hydronium, or H_2O molecules. In the analcite structure, the aluminosilicate tetrahedra link up to form large polyhedra that are occupied by H_2O molecules in analcite, Cs^+ ions in pollucite, or K^+ ions in high leucite (Deer et al., 1963, p. 340). The molecular H_2O contributes 59 J/mol·K H_2O to the molar entropy of analcite at 298 K, which is substantially larger than the typical entropy contribution of 40.2 J/mol·K H_2O as OH in sheet silicates (Helgeson et al., 1978, p. 49) but smaller than the entropy of liquid water at 298 K (69.9 J/mol·K). Inasmuch as interlayer sites in micas provide a somewhat snugger fit than H_2O sites in analcite, the entropy contribution by interlayer molecular H_2O in hydropyrophyllite and micas can be estimated as near 52 ± 4 J/mol·K H_2O, and $\Delta_r S^0 \simeq 52–69.9 = -18$ J/mol·K for the hydration of interlayer vacancies.

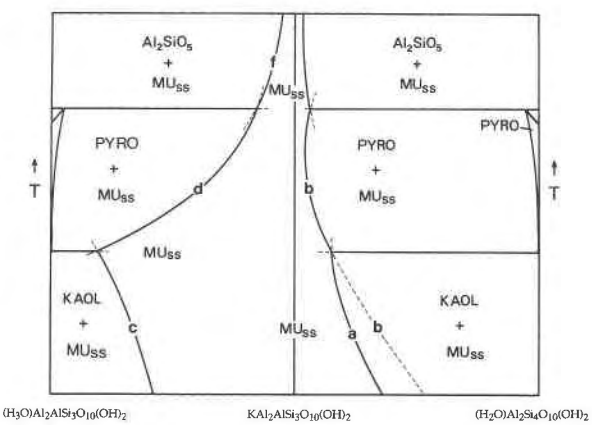

Fig. 4. Schematic representation of topologic relations among illite-muscovite crystalline solution (MU_{SS}) and aluminum silicates (KAOL, kaolinite; PYRO, pyrophyllite) on two faces of the triangular prism temperature-$(H_3O)(Al_2AlSi_3O_{10}(OH)_2$-$KAl_2AlSi_3O_{10}(OH)_2$-$(H_2O)Al_2Si_4O_{10}(OH)_2$. The configurations and relative slopes of the phase boundaries are consistent with qualitative thermodynamic arguments regarding chemical interactions among the mineral components as identified by equilibria a–d and f listed in the text and labeled on the diagram. Quartz and aqueous fluid are present in all assemblages. The field breadth shown for illite-muscovite at lower temperatures is guided somewhat by data in Table 3 and by inference regarding relative nonideality of mixing along the two joins.

The structural transformation from $\square Al_2Si_4O_{10}(OH)_{2,mica}$ to $Al_2Si_4O_{10}(OH)_{2,pyro}$ involves elimination of interlayer sites by a shift of facing tetrahedral sheets along one of the pseudohexagonal axes by about $0.3a$ so that the Si^{4+} cations do not superpose as in micas but are staggered or nested in a way that minimizes Si^{4+}-Si^{4+} repulsion across the interlayer region (Evans and Guggenheim, 1988, p. 229). This translation in stacking 2:1 layers avoids breaking strong chemical bonds, so the entropy of transformation is unlikely to exceed that of the ortho- to clinopyroxene transformation, which involves a glide along (100) with a translation $b/2$ (Deer et al., 1978, p. 22). On the basis of a 20-atom formula like pyrophyllite, the clino → ortho transition has $\Delta_r S^0 \simeq 3.8$ J/mol·K in enstatite and $\Delta_r S^0 \simeq 3.4$ J/mol·K in ferrosilite (Lindsley, 1981) or possibly smaller values (Berman, 1988). The foregoing considerations permit the molar entropy of hydropyrophyllite at 25 °C to be estimated from that of pyrophyllite (239.4 J/mol·K; Berman, 1988) as $S^0_{hydropy} \simeq 291 \pm 3$ J/mol·K.

With reference to thermal decomposition of the hydropyrophyllite component in Figure 4, the entropy change of the reaction $(H_2O)Al_2Si_4O_{10}(OH)_2 = Al_2Si_2O_5(OH)_4 + 2SiO_2$ may be calculated using $S^0 = 203.7$ J/mol·K for kaolinite and $S^0 = 41.5$ J/mol·K for quartz (Berman, 1988), giving $\Delta_r S^0_{298} \cong -4 \pm 4$ J/K, which accords with the intuition that $\Delta_r S^0$ should be negative, because OH is more strongly bonded than molecular H_2O (and held to higher temperature), and that $\Delta_r S$ should be small for a solid-solid reaction. This value of $\Delta_r S$ means this reaction is not responsible for the continuous liberation of H_2O from illite during heating from 100 to 200 °C.

Instead, the pertinent equilibria are Reactions a and b on Figure 4:

$$3(H_2O)Al_2Si_4O_{10}(OH)_2 = 2(H_3O)Al_2AlSi_3O_{10}(OH)_2 + 6SiO_2 + H_2O \quad (a)$$

$$(H_2O)Al_2Si_4O_{10}(OH)_2 = Al_2Si_4O_{10}(OH)_2 + H_2O \quad (b)$$

both of which have positive $\Delta_r S^0$. Because of likely kinetic retardation of Reaction a during rapid heating in the laboratory, the low-temperature metastable extension of Reaction b is the default mechanism that is likely responsible for much of the reported continuous H_2O loss from illite over the 100–200 °C interval.

Diagenesis of kaolinite-bearing sediments, such as those described by Merino and Ransom (1982), should lead to hydronium enrichment in illite with increasing temperature (Table 3) and accompanying kaolinite destruction according to the reaction

$$3Al_2Si_2O_5(OH)_4 = 2(H_3O)Al_2AlSi_3O_{10}(OH)_2 + H_2O. \quad (c)$$

This reaction has positive $\Delta_r S^0$ and so yields maximum activity of the hydromuscovite molecule in white mica at high temperature and low P_{H_2O}, as in boiling-condensing hydrothermal systems or in diagenetic-metamorphic environments with low X_{H_2O}/X_{CO_2}.

The hydromuscovite-pyrophyllite equilibrium

$$2(H_3O)Al_2AlSi_3O_{10}(OH)_2 + 6SiO_2 = 3Al_2Si_4O_{10}(OH)_2 + 2H_2O \quad (d)$$

indicates the opposite; i.e., increase of temperature beyond the kaolinite stability limit into the stability range of pyrophyllite causes progressive decomposition of the hydromuscovite component of the mica in favor of the higher entropy assemblage pyrophyllite + fluid.

For equilibrium among the kaolinite, pyrophyllite, and hydromuscovite components, we have $2Al_2Si_2O_5(OH)_4 + Al_2Si_4O_{10}(OH)_2 = 2(H_3O)Al_2AlSi_3O_{10}(OH)_2 + 2SiO_2$, which indicates, like Reaction d, that elevated silica activity depresses the activity of the hydromuscovite component. Hydromuscovite activity would be maximized in silica-undersaturated assemblages but lower in micas associated with coarse-grained quartz and lower still in association with chalcedony, cristobalite, or opaline silica. This reaction also says that the activity of the hydromuscovite component in white mica solid solution will be maximized when white mica occurs in an assemblage in which the activities of the kaolinite and pyrophyllite components are simultaneously maximized, i.e., in the equilibrium phase assemblage white mica + kaolinite + pyrophyllite (Fig. 4), which forms rather commonly at temperatures near 275–300 °C in hydrothermal alteration assemblages associated with porphyry Cu-Mo deposits, porphyry and lode tin deposits such as those of Cornwall, alunitic epithermal gold deposits of the Comstock Lode type, and metabauxites and marly limestones in the lower greenschist facies. The investigator interested in instrumental studies of hydronium-rich micas may seek suitable sample material in those parageneses.

Isotope studies

The preceding sections have established that H_2O bound in interlayer sites is a substantial fraction of total structural H_2O in most hydrothermal and low-metamorphic grade muscovite samples and even in some pegmatitic micas. DTGA studies of hydromicas by Kodama and Brydon (1968) and by MacKenzie et al. (1949) have found three pulses of dehydration: one below 110 °C, one in the 200–500 °C range, and a third in the 600–700 °C interval. The last is also characteristic of K-rich muscovite and is attributed to dehydroxylation. The first is largely hygroscopic surface H_2O. The second is here interpreted as loss of interlayer molecular H_2O and hydronium over a temperature range that resembles the thermal retentiveness of neutral Ar atoms in micas (which have geochronologic Ar blocking temperatures around 300–500 °C, varying with mica composition and grain size; Dalrymple and Lanphere, 1969). The DTGA curves for interlayer sites must vary with proportions and hence the diffusion rates of H_2O^0, H_3O^+, and K^+, inasmuch as H_2O^0 and H_3O^+ surely have different lattice binding energies, and the pro-

portion of K^+ influences the fraction of remaining interlayer sites through which the more mobile occupants can diffuse and hence influences their diffusion rates. The latter consideration also suggests that the diffusivity of Ar may be significantly greater and the blocking temperature lower in illite and hydrothermal and metamorphic hydromicas than in more potassic muscovite.

The substantial difference in binding energies of H_2O in OH sites and interlayer sites that is indicated by the forementioned H isotope exchange kinetics (Moum and Rosenqvist, 1958) and DTGA studies implies that fractionation factors for O and H isotopes should be very different in the two kinds of lattice sites, by analogy with the strong O isotope fractionation between OH and aluminosilicate oxygen in micas (Hamza and Epstein, 1979; O'Neill, 1986) and the large H isotope fractionation (27‰ δD at 22 °C) between hydronium and OH sites in jarosite (Alpers and Nordstrom, 1988). H_2O extraction procedures that mix contributions from interlayer and OH sites could result in substantially erroneous petrogenetic interpretation. Excess H_2O yield over the true OH yield might go unrecognized if the expected stoichiometric amount were not adjusted to compensate for halogens and naturally deprotonated OH in ferrimicas, based on a complete chemical analysis.

If, as has been demonstrated for hydronium jarosite (Alpers and Nordstrom, 1988), bound interlayer H_2O and hydronium in sericite have characteristic release temperatures that are sufficiently distinct from release temperatures of adsorbed H_2O and from OH or if they can be separately sampled by ion-exchange treatment or low-current microbeam techniques, then stable isotope analyses of separately released H_2O fractions from the two kinds of lattice sites might be useful as an intracrystalline isotope geothermometer. Or, if H_2O or hydronium in interlayer sites undergoes postdepositional isotope exchange with ambient water much faster than H_2O in OH sites, then the discrepancy of intracrystalline isotope thermometry from the independently known crystallization temperature might be calibrated as a cooling-rate speedometer for ore deposits or low-grade metamorphic rocks.

Petrogenetic modeling

Hydronium is a ubiquitous and commonly substantial constituent in micas formed below about 450 °C, and neutral H_2O molecules are an important constituent of micas from low-temperature environments. Following experimental measurement of the thermodynamic properties of the end-member hydromica components $(H_3O)Al_2AlSi_3O_{10}(OH)_2$ and $(H_2O)Al_2Si_4O_{10}(OH)_2$ and their mixing functions with $KAl_2AlSi_3O_{10}(OH)_2$, a variety of phase equilibria involving hydromica components in muscovite should find widespread application for thermodynamic reconstruction of intensive variables in petrogenetic environments. Such equilibria include Reactions a–d of Figure 4 as well as assemblages in which muscovite coexists with diaspore, corundum, potassium feldspar, or an Al_2SiO_5 mineral:

$$2(H_3O)Al_2AlSi_3O_{10}(OH)_2 + 3KAlSi_3O_8 = 3KAl_2AlSi_3O_{10}(OH)_2 + 6SiO_2 + 2H_2O \quad (e)$$

$$2(H_3O)Al_2AlSi_3O_{10}(OH)_2 = 3Al_2SiO_5 + 3SiO_2 + 5H_2O \quad (f)$$

$$2(H_3O)Al_2AlSi_3O_{10}(OH)_2 + 3Al_2O_3 = 6Al_2SiO_5 + 5H_2O \quad (g)$$

$$(H_3O)Al_2AlSi_3O_{10}(OH)_2 = 3AlO(OH) + 3SiO_2 + H_2O. \quad (h)$$

The assemblage diaspore plus quartz is more stable than kaolinite at high pressure and temperatures to about 450 °C. As displaced equilibria in muscovite-bearing assemblages, each of those reactions is a potential P_{H_2O} barometer for low-grade metapelites. If P_{H_2O} were independently known, one of Equilibria a–h might be combined with others in a petrogenetic grid as a sliding-scale geothermobarometer.

In thermodynamic modeling of weathering, diagenetic cementation, and hydrothermal ore precipitation by electrolyte solutions, pH is a crucially important variable that is commonly difficult to reconstruct because of lack of appropriately low-variance mineral assemblages. With a little independent information, the white mica composition may be used as a paleo pH meter. Consider an assemblage containing quartz and sericite. Heating-freezing tests on fluid inclusions in the quartz permit close estimation of precipitation temperature and molality of chloride salts in the hydrothermal solution (Roedder, 1984). If the Na-K ratio is not analyzed directly in the inclusion fluids, it can be calculated from the Na-K ratio in the sericite, using available thermodynamic data for the fluid-mineral ion-exchange reaction, ionization equilibria in the fluid, and mixing functions for Na and K in interlayer sites. The value of aqueous K^+ ion molality obtained from the mica analysis and chloride molality in fluid inclusions may be applied to the equilibrium $(H_3O)Al_2AlSi_3O_{10}(OH)_2 + K^+_{aq} = KAl_2AlSi_3O_{10}(OH)_2 + H_2O + H^+_{aq}$ to calculate pH, utilizing activities of the mica components obtained from the sericite analysis and an equilibrium constant incorporating a $\Delta_f G^0$ of hydronium muscovite—when it becomes available. It might most readily become available by experimental studies of this reaction or of Reactions c–h involving micas of variable composition.

Conclusions

The statistical tests of fit for alternative ways of calculating mica structural formulas indicate that hydronium ion is a substantial interlayer site occupant in white micas formed in acidic to neutral pH environments at temperatures below about 450 °C. A corollary is that the commonly reported apparent stoichiometric excess of octahedral cations over two is largely a fiction resulting from ignoring hydronium in interlayer sites. For the 72 micas in the Appendix 1 data set, the stoichiometries from mod-

els 2 and 3 have a total number of octahedral and tetrahedral ions that remain within 1% of the stoichiometric ideal of 6 in Li-free muscovite. Neutral H_2O molecules occupy a significant fraction of interlayer crystallographic sites in pedogenic and diagenetic illites and some hydrothermal sericites. Recognition that these are widespread, substantial constituents of white micas opens the door to diverse uses of hydromica components in petrologic studies.

Acknowledgments

This work is part of a research program on hydrothermal alteration in ore deposits supported by the U.S. Bureau of Mines through the Indiana Mining and Mineral Resource Research Institute. The presentation benefited from discussions with Edward Young and from reviews of an earlier draft by Darby Dyar, Charles Guidotti, Thomas Hoisch, and an anonymous reviewer. Kim Beckman is thanked for her patience in retyping the manuscript through many revisions. Giovanni Soto and Matt Stuve assisted with preparation of the figures.

References cited

Aagaard, P., and Helgeson, H.C. (1983) Activity/composition relations among silicates and aqueous solutions: II. Chemical and thermodynamic consequences of ideal mixing of atoms on homological sites in montmorillonites, illites, and mixed-layer clays. Clays and Clay Minerals, 31, 207–217.

Aines, R.D., and Rossman, G. R. (1984) Water in minerals? A peak in the infrared. Journal of Geophysical Research, 89, 4059–4071.

Alpers, C.N., and Nordstrom, D.K. (1988) Solid solution properties and deuterium fractionation factors for hydronium-bearing jarosites from acid mine waters. Eos, 69, 1480.

Baldelli, C., Franceschelli, M., Leoni, L., and Memmi, I. (1989) Ferrimuscovite and celadonite substitutions in muscovite from Fe^{3+}-rich low-grade psammitic rocks (Northern Apennines, Italy). Lithos, 23, 201–208.

Barker, D.S. (1964) Ammonium in alkali feldspars. American Mineralogist, 49, 851–858.

Barrer, R.M., and Denny, P.J. (1961) Hydrothermal chemistry of the silicates. Part IX. Nitrogenous aluminosilicates. Journal of the Chemical Society, 971–983.

Berman, R.G. (1988) Internally consistent thermodynamic data for minerals in the system Na_2O-K_2O-CaO-MgO-FeO-Fe_2O_3-SiO_2-TiO_2-H_2O-CO_2. Journal of Petrology, 29, 445–522.

Bevington, P.R. (1969) Data reduction and error analysis for the physical sciences, 336 p. McGraw-Hill, New York.

Brammall, A., Leech, J.G.C., and Bannister, F.A. (1937) The paragenesis of cookeite and hydromuscovite associated with gold at Ogofau, Carmarthenshire. Mineralogical Magazine, 24, 507–519.

Brown, G., and Norrish, K. (1952) Hydrous micas. Mineralogical Magazine, 29, 929–932.

Butler, B.C.M. (1967) Chemical study of minerals from the Moine schists of the Ardnamurchan area, Argyllshire, Scotland. Journal of Petrology, 8, 233–267.

Dalrymple, G.B., and Lanphere, M.A. (1969) Potassium-argon dating, 258 p. W. H. Freeman, San Francisco.

Deer, W.A., Howie, R.A., and Zussman, J. (1963) Rock-forming minerals, vol. 4: Framework silicates, 435 p. Longman, London.

——— (1978) Rock-forming minerals, vol. 2A: Single-chain silicates (2nd edition), 667 p. Wiley, New York.

Dyar, M.D. (1988) Direct evidence of hydronium substitution in biotite. Geological Society of America Abstracts with Programs, 20, A102.

Erd, R.C., White, D.E., Fahey, J.J., and Lee, D.E. (1964) Buddingtonite, an ammonium feldspar with zeolitic water. American Mineralogist, 49, 831–850.

Ernst, W.G. (1963) Significance of phengitic micas from low-grade schists. American Mineralogist, 48, 1357–1373.

Essene, E.J. (1982) Geologic thermometry and barometry. In Mineralogical Society of America Reviews in Mineralogy, 10, 153–206.

——— (1989) The current status of thermobarometry in metamorphic rocks. In J.S. Daly, R.A. Cliff, and B.W.D. Yardley, Eds., Evolution of metamorphic belts. Geological Society of America Special Publication, 43, 1–44.

Eugster, H.P., and Wones, D.R. (1962) Stability relations of the ferruginous mica, annite. Journal of Petrology, 3, 85–125.

Evans, B.W., and Guggenheim, S. (1988) Talc, pyrophyllite, and related minerals. In Mineralogical Society of America Reviews in Mineralogy, 19, 225–294.

Foster, M.D. (1964) Water content of micas and chlorites. U.S. Geological Survey Professional Paper, 474-F, F1–F15.

Frondel, C. (1970) Colloform hydrothermal muscovite ("chacaltaite"). American Mineralogist, 55, 1437–1440.

Garrells, R.M. (1984) Montmorillonite/illite stability diagrams. Clays and Clay Minerals, 32, 16–166.

Giggenbach, W.F. (1985) Construction of thermodynamic stability diagrams involving dioctahedral potassium clay minerals. Chemical Geology, 49, 231–242.

Guggenheim, S., Chang, Y.-H., and Koster van Groos, A.F. (1987) Muscovite dehydroxylation: High temperature studies. American Mineralogist, 72, 537–550.

Guidotti, C.V. (1984) Micas in metamorphic rocks. In Mineralogical Society of America Reviews in Mineralogy, 13, 357–468.

Hallam, M., and Eugster, H.P. (1976) Ammonium silicate stability relations. Contributions to Mineralogy and Petrology, 57, 227–244.

Hamza, M., and Epstein, S. (1979) Oxygen isotope fractionation between oxygen of different sites in hydroxyl-bearing silicate minerals. Geochimica et Cosmochimica Acta, 44, 173–182.

Helgeson, H.C., and Aagaard, P. (1985) Activity composition relations among silicates and aqueous solutions. I. Thermodynamics of intrasite mixing and substitutional order/disorder in minerals. American Journal of Science, 285, 769–844.

Helgeson, H.C., Delaney, J.M., Nesbitt, H.W., and Bird, D.K. (1978) Summary and critique of the thermodynamic properties of rock-forming minerals. American Journal of Science, 278-A, 1–229.

Hervig, R.L., and Peacock, S.M. (1989) Water and trace elements in coexisting muscovite and biotite from metamorphic rocks. Eos, 70, 490.

Higashi, S. (1982) Tobelite, a new ammonium dioctahedral mica. Mineralogical Journal, 11, 138–146.

Hofmeister, A.M., and Rossman, G.R. (1985) A spectroscopic study of irradiation coloring of amazonite: Structurally hydrous, Pb-bearing feldspar. American Mineralogist, 70, 794–804.

Holdaway, M.J. (1980) Chemical formulae and activity models for biotite, muscovite, and chlorite applicable to pelitic metamorphic rocks. American Mineralogist, 65, 711–719.

Honma, H., and Itihara, Y. (1981) Distribution of ammonium in minerals of metamorphic and granitic rocks. Geochimica et Cosmochimica Acta, 45, 983–988.

Hori, H., Nagashima, K., Yamada, M., Miyawaki, R., and Marubashi, T. (1986) Ammonioleucite, a new mineral from Tatarazawa, Fujioka, Japan. American Mineralogist, 71, 1022–1027.

Hower, J., and Mowatt, T.C. (1966) The mineralogy of illites and mixed-layer illite/montmorillonites. American Mineralogist, 51, 825–854.

Hunziker, J.C., Frey, M., Clauer, N., Dallmeyer, R.D., Friedrichsen, H., Flehmig, W., Hochstrasser, K., Roggwiler, P., and Schwander, H. (1986) The evolution of illite to muscovite: Mineralogical and isotopic data from the Glarus Alps, Switzerland. Contributions to Mineralogy and Petrology, 92, 157–180.

Ito, S., Kubo, N., Nariki, S., and Yoneda, N. (1987) Ion exchange in alkali layers of potassium β-ferrite ($(1 + x)K_2O \cdot 11Fe_2O_3$) single crystals. Journal of the American Ceramic Society, 70, 874–879.

Jiang, W.-T., Essene, E.J., and Peacor, D.R. (1990) Transmission electron microscopic study of coexisting pyrophyllite and muscovite: Direct evidence for the metastability of illite. Clays and Clay Minerals, 38, 225–240.

Keren, R., and Shainberg, I. (1975) Water vapor isotherms and the heat of immersion of Na/Ca-montmorillonite systems—I: Homoionic clay. Clays and Clay Minerals, 23, 193–200.

Kodama, H., and Brydon, J.E. (1968) Dehydroxylation of microcrystalline muscovite. Transactions of the Faraday Society, 64, 3112–3119.

Lambert, R.St.J. (1959) The mineralogy and metamorphism of the Moine

schists of the Morar and Knoydart districts of Inverness-shire. Transactions of the Royal Society of Edinburgh, 63, 553–588.

Lindsley, D.H. (1981) The formation of pigeonite on the join hedenbergite-ferrosilite at 11.5 and 15 kbar: Experiments and a solution model. American Mineralogist, 66, 1175–1182.

Lippmann, F. (1982) The thermodynamic status of clay minerals. In H. van Olphen and F. Veniale, Eds., Proceedings of the Seventh International Clay Conference, 1981, Bologna, Italy, p. 475–485. Elsevier, New York.

Ludington, S.D. (1978) The biotite-apatite thermometer revisited. American Mineralogist, 63, 551–553.

Lundgren, J.-O., and Olovsson, I. (1976) The hydrated proton in solids. In P. Schuster, G. Zundel, and C. Sandorfy, Eds., The hydrogen bond. II. Structure and spectroscopy, p. 471–526. North-Holland, Amsterdam.

Mackenzie, R.C., Walker, G.F., and Hart, R. (1949) Illite occurring in decomposed granite at Aberdeenshire. Mineralogical Magazine, 28, 704–713.

Merino, E., and Ransom, B. (1982) Free energies of formation of illite solid solutions and their compositional dependence. Clays and Clay Minerals, 30, 29–39.

Moum, J., and Rosenqvist, I.Th. (1958) Hydrogen (protium)-deuterium exchange in clays. Geochimica et Cosmochimica Acta, 14, 250–252.

Munoz, J.L., and Ludington, S.D. (1974) Fluorine-hydroxyl exchange in biotite. American Journal of Science, 274, 396–413.

Neiva, A.M.R. (1975) Geochemistry of coexisting aplites and pegmatites and of their minerals from central northern Portugal. Chemical Geology, 16, 153–177.

Nemec, D. (1980) Fluorine phengites from tin-bearing orthogneisses of the Bohemian-Moravian Heights, Czechoslovakia. Neues Jahrbuch für Mineralogie, 139, 155–169.

Newman, A.C.D., and Brown, G. (1987) The chemical constitution of clays. In A.C.D. Newman, Ed., Chemistry of clays and clay minerals, vol. 6, p. 1–128. Wiley, New York.

Norrish, K., and Pickering, J.G. (1983) Clay minerals. Soils: An Australian viewpoint, p. 281–308. Academic Press, London.

O'Neill, J.R. (1986) Theoretical and experimental aspects of isotopic fractionation. In Mineralogical Society of America Reviews in Mineralogy, 16, 1–40.

Peck, L.C. (1964) Systematic analysis of silicates. U.S. Geological Survey Bulletin, 1170, 89 p.

Ripmeester, J.A., Ratcliffe, C.I., Dutrizac, J.E., and Jambor, J.L. (1986) Hydronium ion in the alunite-jarosite group. Canadian Mineralogist, 24, 435–447.

Roedder, E. (1984) Fluid inclusions. In Mineralogical Society of America Reviews in Mineralogy, 12, 644 p.

Sclar, C.B., Carrison, L.C., and Schwartz, C.M. (1965) High-pressure synthesis of a new hydronium-bearing layer silicate in the system MgO-SiO_2-H_2O. Transactions of the American Geophysical Union, 46, 184.

Środoń, J., and Eberl, D.D. (1984) Illite. In Mineralogical Society of America Reviews in Mineralogy, 13, 495–544.

Sterne, E.J., Reynolds, R.C., Jr., and Zantop, H. (1982) Natural ammonium illites from black shales hosting a stratiform base metal deposit, Delong Mountains, northern Alaska. Clays and Clay Minerals, 30, 161–166.

Stoessel, R.K. (1981) Refinements in a site-mixing model for illites: Local electrostatic balance and the quasi-chemical approximation. Geochimica et Cosmochimica Acta, 45, 1733–1741.

Sudo, T. (1978) An outline of clays and clay minerals in Japan. Developments in Sedimentology, 26, 1–103.

Tardy, Y., and Fritz, B. (1981) An ideal solid solution model for calculating solubility of clay minerals. Clay Minerals, 16, 361–373.

Till, R. (1974) Statistical methods for the earth scientist: An introduction, 154 p. Wiley, New York.

Wang, G.-F., and Banno, S. (1987) Non-stoichiometry of interlayer cations in micas from low- to middle-grade metamorphic rocks in the Ryoke and the Sanbagawa belts, Japan. Contributions to Mineralogy and Petrology, 97, 313–319.

Weaver, C.E., and Pollard, L.D. (1973) The chemistry of clay minerals. Developments in Sedimentology, 15, 213 p.

White, J.L., and Burns, A.F. (1963) Infrared spectra of hydronium ion in micaceous minerals. Science, 141, 800–801.

Wilkins, R.W.T., Mateen, A., and West, G.W. (1974) The spectroscopic study of oxonium ions in minerals. American Mineralogist, 59, 811–819.

Williams, J.M. (1976) Spectroscopic studies of hydrated proton species, $H^+(H_2O)_n$, in crystalline compounds. In P. Schuster, G. Zundel, and C. Sandorfy, Eds., The hydrogen bond. II. Structure and spectroscopy, p. 655–682. North-Holland, Amsterdam.

Wise, W.S., and Eugster, H.P. (1964) Celadonite: Synthesis, thermal stability and occurrence. American Mineralogist, 49, 1031–1083.

Zen, E-An (1981) Metamorphic mineral assemblages of slightly calcic pelitic rocks in and around the Taconic allochthon, southwestern Massachusetts and adjacent Connecticut and New York. U.S. Geological Survey Professional Paper 1113, 128 p.

Manuscript received October 6, 1989
Manuscript accepted May 20, 1991